Recent Developments in Graphene-based Optical Modulators

Ran Hao, J. M. Jin, and E. P. Li
Department of Information Science and Electronics Engineering
Zhejiang University, Hangzhou 310027, China
(*Invited Paper*)

Abstract— Graphene has shown promising perspectives in optical active components due to the large active-control of its permittivity-function. This paper systematically reviews the recent developments of graphene-based optical modulators, including material property, single-layer, multi-layer, few-layer graphene-based modulator and corresponding figure-of-merits. The results showed graphene is an excellent material for enhancing silicon's weak modulation capability after it is integrated into the silicon platform, showing significant influence on optical interconnects in future integrated optoelectronic circuits.

1. INTRODUCTION

Optical modulator is a device which is used to modulate (alter) the properties of a light such as amplitude, phase or polarization by electro-refraction (ER) or electro-absorption (EA) modulation. The electric effects that traditionally cause either ER or EA are Pockels effect, Kerr effect, Franz-Keldysh effect and plasma dispersion effect [1]. However, these effects are too weak in pure silicon material at the communication wavelengths so that it usually needs an extremely large arm length which results in large footprint as well as high drive voltage to reach the required modulation [9]. In addition, the side-effect introduced to the pass-band and stability after applying some enhancement methods is still challenging. Even with the doping of silicon, the modulation speed is limited due to the low carrier mobility in silicon, e.g., the best reported modulation speed is up to 50 Gbit/s and difficult to be further improved [2]. To overcome these fundamental bottlenecks, novel materials need to be explored so that they can provide better modulation capability and CMOS compatibility simultaneously. Graphene has attracted lots of interest due to its remarkable mechanical, electric, magnetic thermal and optical properties [6]. The unique properties of graphene such as strong coupling with light, high-speed operation, and gate-variable optical conductivity make it a very promising material for optical modulators [1]. When the imaginary part of graphene conductivity is negative, graphene supports the transverse magnetic mode noted as surface plasmon polaritons (SPP) [4], displaying potential applications for highly tunable SPP modulator applications [5]. This is why a large amount of research attention has been focused on the graphene-based optical modulator [11].

In this paper, we systematically reviewed the mechanism and recent developments for various graphene-based electro-refraction (ER) modulators.

2. OPTICAL MATERIAL PROPERTIES OF SINGLE-LAYER GRAPHENE

Figure 1 shows the 3D graphene permittivity introduced by Vakil and Engheta, and the conductivity of an infinite graphene sheet with a thickness of 0.7 nm at the wavelength $\lambda = 1550$ nm which is computed from the Kubo formula [4, 7]. It can be seen that there is a dip in the curve of permittivity magnitude, and the epsilon-near-zero (ENZ) point is obtained at the chemical potential $\mu_{c0} = 0.513$ eV where the absolute value of epsilon is approaching zero. When the chemical potential $\mu_c < \mu_{c0}$, both the real and imaginary part of the permittivity ($\mathrm{Re}(\varepsilon_{//})$ and $\mathrm{Im}(\varepsilon_{//})$) have the positive sign so that the graphene layer behaves like a dielectric material. When the chemical potential is gradually increased, the "dielectric graphene" is gradually transforming into "metallic graphene" at the transition chemical potential $\mu_{c0} = 0.513$ eV. There exists a range where in which both $\mathrm{Re}(\varepsilon_{//})$ and $\mathrm{Im}(\varepsilon_{//})$ are very close to zero called ENZ point. When $\mu_c > 0.52$ eV, $\mathrm{Re}(\varepsilon_{//})$ becomes negative and $\mathrm{Im}(\varepsilon_{//})$ is approaching zero which means the graphene layer acts like a metallic layer, and the graphene layer is then fabulous to transfer surface plasmon polaritons (SPP) [10], displaying much more potential for future optoelectronic devices.

3. SINGLE-LAYER GRAPHENE-BASED MODULATOR

The effective modal refractive index (n_{eff}) of the graphene-embedded silicon waveguide (GESW, as depicted in Fig. 2(a)) is the critical parameter that determines the overall GESW properties. The

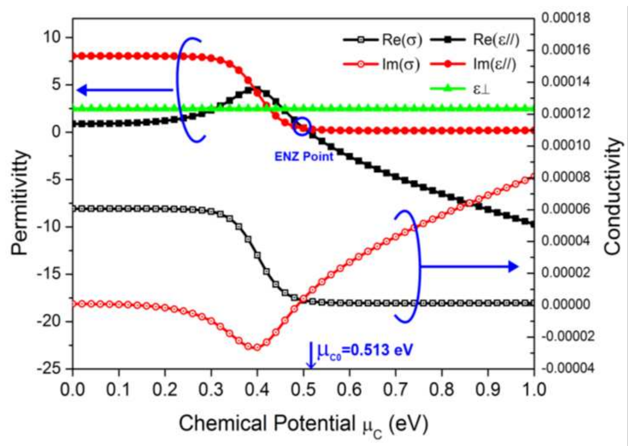

Figure 1: Conductivity and permittivity of an infinite graphene sheet (the wavelength is fixed at 1550 nm) (reprinted from Ref. [5]).

real part of the index ($\mathrm{Re}(n_{\mathrm{eff}})$) is linear to mode's phase information via: $\varphi = k_0\mathrm{Re}(n_{\mathrm{eff}})L$, where k_0 is the wave number in vacuum and L is the propagation distance. The imaginary part of the index ($\mathrm{Im}(n_{\mathrm{eff}})$) is related to the propagation loss α through $\alpha = 8.68k_0\mathrm{Im}(n_{\mathrm{eff}})$ [5]. Therefore, the configuration of an optical modulator can be implement by changing either the $\mathrm{Re}(n_{\mathrm{eff}})$ or $\mathrm{Im}(n_{\mathrm{eff}})$: the former one is typically the phase modulator, while the later one is amplitude modulator. The calculated $\mathrm{Re}(n_{\mathrm{eff}})$ and the $\mathrm{Im}(n_{\mathrm{eff}})$ for the proposed GESW under the chemical potential from 0 to 1 eV is shown as Fig. 2(b). According to the modal theory, the n_{eff} is then calculated from

$$n_{\mathrm{eff}} = \frac{\zeta}{k_0} = \frac{\beta}{k_0} + i\frac{\delta_z}{k_0}, \quad (1)$$

where ζ is the eigenvalue of the system, β is the propagation constant, and δ_z is the attenuation constant. In Fig. 2(b), the n_{eff} of the proposed waveguide is lower than silicon's refractive index (3.45) at all chemical potentials. An inflection point is observed in the $\mathrm{Re}(n_{\mathrm{eff}})$ curve at $\mu_c = 0.4$ eV, where n_{eff} changes intensively near the inflection point. If comparing Fig. 2(b) with Fig. 1, a similarity between the n_{eff} curve and graphene's $\varepsilon_{//}$ curve can be found. It is thus inferred that n_{eff} is proportional with $\varepsilon_{//}$, and one could control n_{eff} to the desired value in terms of simply changing n_{eff}.

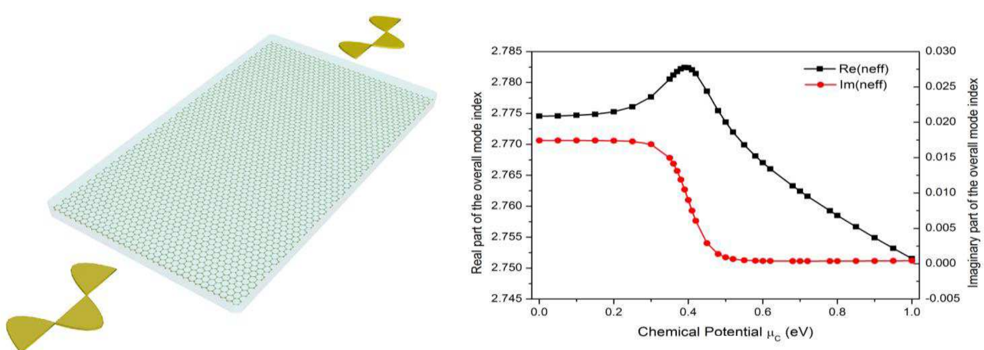

Figure 2: (a) 3D view of GESW; (b) real and imaginary parts of effective modal index variation under different chemical potentials for GESW (reprinted from Ref. [5]).

The impressive large value of Δn_{eff} is great appreciated for the modulator designs based on ER effect, such as MZ modulator, as shown in the schematic picture of Fig. 3(a). Let us first fix one chemical potential at $\mu_{c1} = 1$ eV. With μ_{c2} changing, the corresponding Δn_{eff} will be modified, thus the required arm length L_π to reach the π phase shift is modified. The propagation loss can be evaluated in terms of the maximum allowed length $L_{\max}$ as shown in the red curve in Fig. 3(b), indicating the length where the energy at the output decays to $1/e$ of its original value. We would

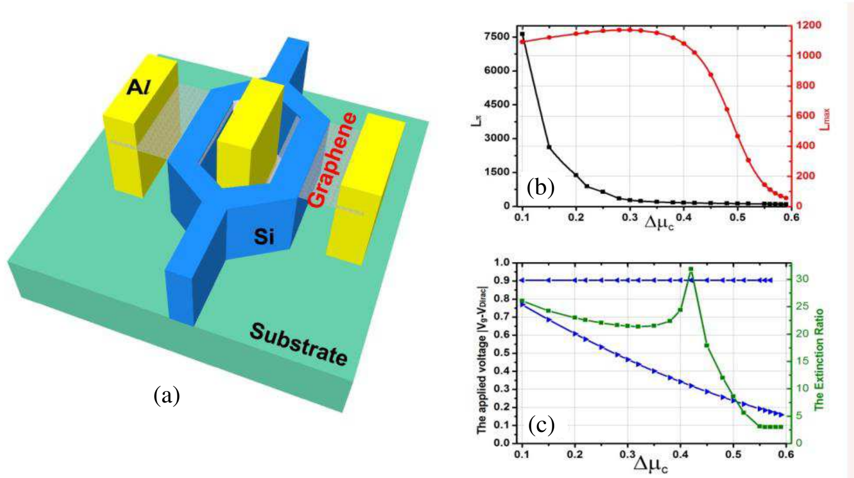

Figure 3: (a) Schematic pictures for top view of the MZ modulator configuration; (b) relationship between $L_\pi/L_{\max}$ and μ_c; (c) relationship between the applied votages/extinction ratio and μ_c.

focus our attention on the condition that $L_\pi < L_{\max}$ in which case the waveguide has enough power at the output [5]. When $\Delta\mu_c = 0.3\,\text{eV}$, L_π is 120 μm, which is one order of magnitude smaller than the present reported value [3]. If the width of the modulation arm is 450 nm and the distance between the two arms is 1.7 μm. Taking into account of the electrode width of 1 μm on each arm side, the overall width of the device is 5 μm. thus the footprint of our proposed modulator is only 120 μm × 5 μm [5]. This small size as well as the CMOS compactable structure indicates its valuable capability to be integrated into photonic circuits in a single chip.

Another important parameter for the MZ modulator is the applied voltage V_g. The blue curves in Fig. 3(c) have shown the difference between V_{g1} (for signal "1" of the reference arm) and V_{g2} (for signal "0" of the modulated arm) is called π shift voltage V_π. As expected. Since L_π decreases much faster than the increase speed of V_π, the minimum modulation efficiency $V_\pi L_\pi$ would be achieved at $55\,\text{V} \cdot \mu\text{m}$ where L_π is smallest at 120 μm. One significant advantage for MZ modulator is that the extinction ratio is high if compared with EA modulators. Fig. 3(c) shows the extinction ratio and applied voltage V_g variations with μ_c, where a maximum extinction ratio of 34 dB has been observed at $\Delta\mu_c = 0.42\,\text{eV}$.

4. MULTI-LAYER GRAPHENE-BASED MODULATOR

4.1. Multi-layer Graphene-based Modulator

Multi-layer graphene based devices have also been studied for the modulator application. Based on the above monolayer graphene-embedded modulator, it is straightforward to embed the multi-layer graphene sheets inside silicon waveguide. An eight-layer graphene embedded MZ modulator [5] is shown in Fig. 4(a). The corresponding electric field distribution in one of the arm of modulator is shown in Fig. 4(b). As demonstrated previously, the field profile displays a Gaussian-like distribution. It has been theoretically demonstrated that by embedding multi-layer graphene in the silicon waveguide, the Δn_{eff} has been increased significantly under the same chemical potential change compared with the monolayer graphene. Therefore, the L_π has been reduced to 27.57 μm which means a much smaller arm length is needed to acquire the π phase shift, as shown in Fig. 4(c). The overall footprint is then estimated as 5 μm × 30 μm. Moreover, the proposed graphene embedded modulator is highly tunable whose overall modal index is in linear relationship with the in-plane permittivity of graphene. The high modulation efficiency is further optimized to $20\,\text{V} \cdot \mu\text{m}$, which is 6 times better than the monolayer case. In Fig. 4(d), The extinction ratio is 35 dB at smaller arm length compared with Fig. 3.

4.2. Few-layer Graphene-based Modulator

Previous discussion on multi-layer graphene relies on the fact that graphene sheets are inserted into the silicon waveguide individually, separated with a distance between the adjacent sheets. However, this scheme adds the difficulties in fabrication and the modulation efficiency. There is an alternative way to embed an N-layer thick graphene sheet in the silicon waveguide. Particularly, when the number of layer $N < 5$, it is called few-layer graphene that exhibits even better performance than

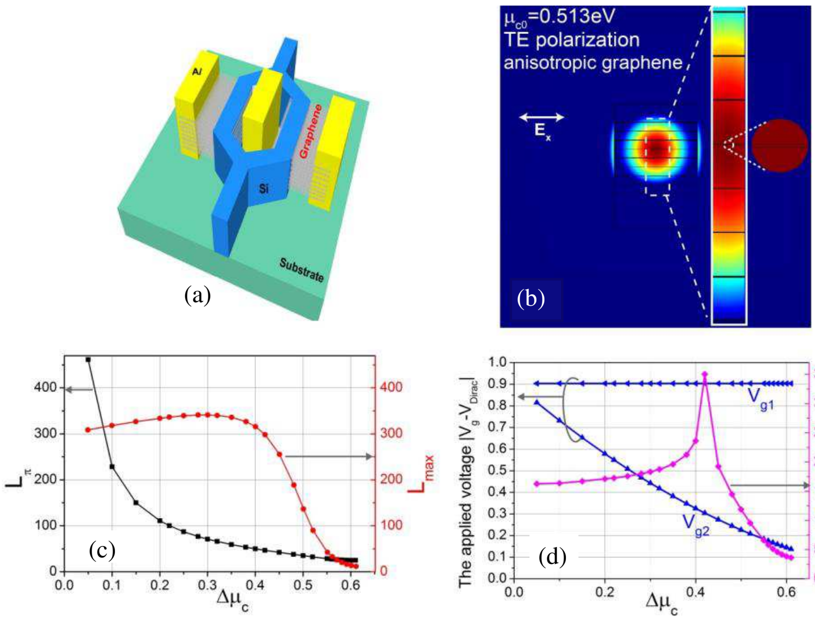

Figure 4: (a) Schematic pictures for eight-layer graphene embedded MZ modulator configuration; (b) corresponding electric field distribution in one of the arm; (c) relationship between $L_\pi L_{\max}$ and $\Delta\mu_c$; (d) relationship between the applied votages/extinction ratio and $\Delta\mu_c$ (reprinted from Ref. [5]).

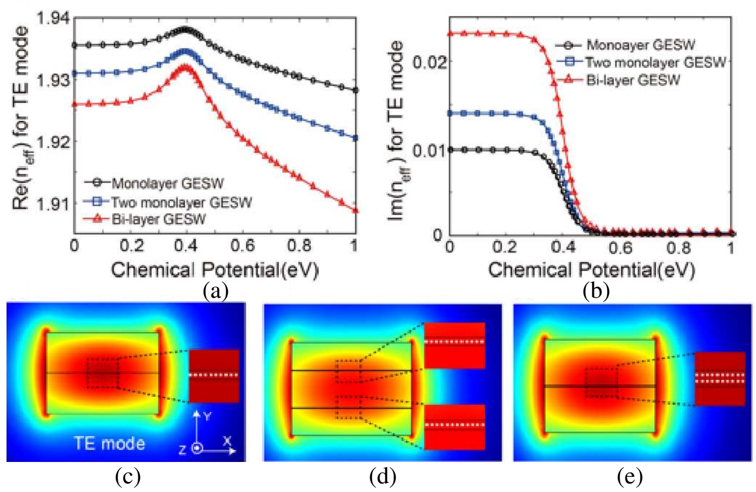

Figure 5: (a) Re(neff) with chemical potential variation for monolayer, two separated monolayer, and bi-layer GESW; (b) Im(neff) with chemical potential variation for monolayer, two separated monolayer, and bi-layer GESW; (c) (d) and (e) represent the electric field distribution for TE polarization mode of monolayer, two separated monolayer, and bi-layer GESW under chemical potential of 0 eV, respectively.

the monolayer graphene.

The effective mode index curves for monolayer GESW, two separated monolayer GESW, and bi-layer GESW are plotted in Figs. 5(a) and 5(b). First, the variation of $\mathrm{Re}(n_{\mathrm{eff}})$ for the bi-layer GESW is roughly two times of the monolayer GESW as expected. However, the variation of $\mathrm{Re}(n_{\mathrm{eff}})$ for the bi-layer GESW is much larger than that of the two separated monolayer GESW, which implies the light-matter interaction between light and bi-layer graphene is much more pronounced compared to that of the two separated monolayer graphene. Secondly, these three curves have basically the same variation trend, namely, it first increases to a maximum value (around the chemical potential of 0.4 eV) and then decreases to the minimum value (at the chemical potential of 1 eV). Therefore, a large Δn_{eff} can be obtained when chemical potential is between 0.4 and 1 eV. To show the difference, the typical electric field modal profiles for monolayer, two separated monolayer, and bi-layer GESW under chemical potential of 0 eV are plotted in Figs. 5(c)–5(e), respectively.

5. CONCLUSION

In conclusion, we reviewed recent progress in graphene-based electro-refraction (ER) modulators. By embedding the graphene sheet into the silicon waveguide, the light-matter interaction has been significantly enhanced: the overall mode index, $\mathrm{Re}(n_{\mathrm{eff}})$ and $\mathrm{Im}(n_{\mathrm{eff}})$, are linked to the in-plane permittivity of the embedded graphene and the n_{eff}variation of GESW can be orders of magnitude larger than silicon waveguide. The modulators based on single-layer graphene, bi-layer graphene, eight-layer graphene, and few-layer graphene were investigated and categorized. It can be concluded that graphene is a very promising material for enhancing the modulation effect in silicon, and has great potentials for future CMOS compatible high efficiency optical modulator, showing significant influence for optical interconnects in future integrated optoelectronic systems.

REFERENCES

1. Liu, M., X. Yin, E. Ulin-Avila, B. Geng, T. Zentgraf, L. Ju, F. Wang, and X. Zhang, "A graphene-based broadband optical modulator," *Nature*, Vol. 474, No. 7349, 64–67, 2011.
2. Tu, X., T. Y. Liow, J. Song, X. Luo, Q. Fang, M. Yu, and G. Q. Lo, "50-Gb/s silicon optical modulator with traveling-wave electrodes," *Optics Express*, Vol. 21, No. 10, 12776–12782, 2013.
3. Thomson, D., F. Y. Gardes, J. M. Fedeli, S. Zlatanovic, Y. Hu, B. P. P. Kuo, E. Myslivets, N. Alic, S. Radic, G. Z. Mashanovich, and G. T. Reed, "50-Gb/s silicon optical modulator," *IEEE Photonics Technology Letters*, Vol. 24, No. 4, 234–236, 2012.
4. Vakil, A. and N. Engheta, "Transformation optics using graphene," *Science*, Vol. 332, No. 6035, 1291–1294, 2011.
5. Hao, R., W. Du, H. Chen, X. Jin, L. Yang, and E. Li, "Ultra-compact optical modulator by graphene induced electro-refraction effect," *Applied Physics Letters*, Vol. 103, No. 6, 061116, 2013.
6. Ju, L., B. Geng, J. Horng, C. Girit, M. Martin, Z. Hao, H. A. Bechtel, X. Liang, A. Zettl, Y. R. Shen, and F. Wang, "Graphene plasmonics for tunable terahertz metamaterials," *Nature Nanotechnology*, Vol. 6, No. 10, 630–634, 2011.
7. Gusynin, V. P., S. G. Sharapov, and J. P. Carbotte, "Magneto-optical conductivity in graphene," *Journal of Physics: Condensed Matter*, Vol. 19, No. 2, 026222, 2007.
8. Du, W., R. Hao, and E. P. Li, "The study of few-layer graphene based Mach-Zehnder modulator," *Optics Communications*, Vol. 323, 49–53, 2014.
9. Hao, R., E. Li, and X. Wei, "Two-dimensional light confinement in cross-index-modulation plasmonic waveguides," *Optics Letters*, Vol. 37, No. 14, 2934–2936, 2012.
10. Lee, C. C., S. Suzuki, W. Xie, and T. R. Schibli, "Broadband graphene electro-optic modulators with sub-wavelength thickness," *Optics Express*, Vol. 20, No. 5, 5264–5269, 2012.
11. Barnes, W. L., A. Dereux, and T. W. Ebbesen, "Surface plasmon subwavelength optics," *Nature*, Vol. 424, No. 6950, 824–830, 2003.